Journal of Electrical Bioimpedance
www.bioimpedance.net

J Electr Bioimp, vol. 8, pp. 66-78, 2017
Received 19 Jul 2016 / published 23 Jul 2017
https://doi.org/10.5617/jeb.3350

Review Paper

Spatial resolution in electrical impedance tomography: A topical review

Venkatratnam Chitturi [1, 3] and Nagi Farrukh [2]

1. *Department of Instrumentation Technology, GSSSIETW, Mysuru, India*
2. *Department of Mechanical Engineering, UniTEN, Selangor, Malaysia*
3. *E-mail any correspondence to: cratnamhere@gmail.com*

Abstract

Electrical impedance tomography (EIT) is a relatively new imaging technique. It has the advantages of low cost, portability, non-invasiveness and is free from radiation effects. So far, this imaging technique has shown satisfactory results in functional imaging. However, it is not yet fully suitable for anatomical imaging due to its poor spatial resolution. In this paper, we review the basic directions of research in the area of the spatial resolution of the EIT systems. The improvements to the hardware and the software developments are highlighted. Finally, possible techniques to enhance the spatial resolution of the EIT systems using array processing beamforming methods are discussed.

Keywords: Array processing, current patterns, data acquisition, direct algorithms, EIT hardware, electrodes, fusion techniques, iterative algorithm

Introduction

The word ‘tomograph’ is a combination of the Greek words ‘tomo’, meaning to slice and ‘graph’, meaning image. In 1826, a Norwegian physicist published the concept of tomography for the first time for an object with axi-symmetrical geometry [1]. The word ‘tomography’ implies a cross-sectional image of a particular object. Several tomographic techniques are available nowadays, such as, computed tomography (CT), gamma-ray tomography, x-ray tomography, ultrasonic imaging and magnetic resonance imaging (MRI). The aforementioned techniques are expensive, invasive and not safe. Most of these techniques consume extensive contact time which implies that continuous measurements would be impractical [2].

Electrical impedance tomography (EIT) is a relatively new imaging technology. A general block diagram of an EIT system is shown in Fig. 1.

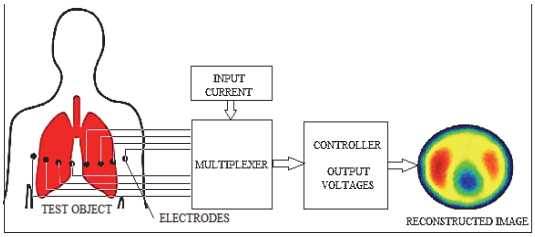

Fig. 1: General block diagram of an EIT system. The input current is injected through a pair of electrodes attached to the test object. The corresponding output voltages are measured and finally an image of conductivity distribution is reconstructed.

Very small currents in terms of ‘mA’ at low frequency are applied to study the electrical properties of the tissues from the measured voltages [3]. This technique is beneficial for its safe use, inexpensiveness, non-invasiveness and portability. It is also suitable for long term monitoring of the test object.

These advantages have helped establish EIT as a functional imaging tool, for example, in monitoring heart and lung function. Other applications include monitoring internal bleeding, emptying of the stomach, pelvic fluid accumulation, local internal temperature changes associated with hyper-thermic treatments and the study of breast cancer to name a few [4]. However, EIT is not fully suitable for anatomical imaging because of its poor spatial resolution.

Background principles

Spatial resolution is an important criterion used in analyzing images generated by EIT imaging systems. Spatial resolution is defined as the number of pixels utilized in the construction of a digital image [5]. An image generated by an EIT system with low spatial resolution is of less importance. Thus, an improvement of the spatial resolution in EIT systems is very important. Currently, EIT systems suffer from low spatial resolution for the following reasons [6].

a) Low relative resolution of measurable data. When the measured data has low resolution compared with their own size, the reconstructed image has low spatial resolution. The data acquisition is highly uncertain and non-linear; hence, an ideal measurement of the data is impractical.
b) Low signal-to-noise ratio. Use of low current excitation causes weak voltage measurements. Also, a small change in the variable leads to a large measurement error. This condition is called soft-field effect. For every soft-field condition, the resolution for the spatial reconstruction is relatively poor due to two reasons:
    i. The fringe effect that is due to the extension of the electric field. The effect mainly occurs within a sensing region, which is not constrained within the electrode plane, but extends also to a volume away from this region. This effect is worse for smaller electrodes. Although they have found that this can be minimized by using a larger volume of electrodes, they observed that this causes EIT systems to lose their local character of measurements. They also found out that it can still be used for monitoring average features of spatially homogenous flows. However, this alternative cannot be used for non-homogenous flows because the measuring volumes should be as narrow as possible to get accurate information. It is difficult to have countermeasures for this effect because there has not yet been actual studies of the cause of the fringe effect over distances between dispersed non-conductive objects and the measuring plane.
    ii. The topography of the field strength at any point inside the measuring volume is a function of the distribution of electrical properties throughout this volume, which causes image reconstruction problems. The problem arises due to low frequencies and the accompanying relatively long wavelength of the electromagnetic radiation. Therefore it affects both the size and physical properties of the components and the objects inside the volume [7].

    Further, the soft field effect makes the EIT imaging process complicated and difficult since an increment of the measuring data has to respond to all pixel variants and is thus a major reason for the low resolution and unstable EIT imaging results in practice. Since the number of measured data is much less than the number of imaging units, the existing EIT algorithms depend on solving a mathematically ill-posed equation. A small amount of noise mixed with the measured data can cause very large errors, thereby making the EIT systems less robust [6].
c) Imaging algorithm. Choosing an algorithm suitable for high spatial resolution is often a challenging problem. Since, the reconstructed images do not have understand-ability or interpretability, these problems are overcome by practical solutions such as simulations and visuali-zation. However, these methods are not practically feasible in reality.

Spatial resolution in early EIT systems

The first electrical impedance images of the thorax using an impedance camera was built using an array of 144 mutually guarded electrodes of very low spatial resolution. A weak electrical signal in the form of a voltage was used to study the electrical properties (impedance) of the tissues. The low spatial resolution was due to the resistances of the electrodes. The electrode resistance was added to the resistance of the material under examination causing a measurement error. Guarded electrodes were used for high resistance tissues, but only when the current was assumed to travel in straight lines. The method used a constant voltage source and measured the variable currents. It was only the magnitude of the admittance that was considered for the reconstruction of the images of the thorax [8].

In contrast, a computed tomography system with input current and output voltages was designed. The resolution of the images was enhanced by increasing the number of layers of the electrodes, as the injected current was not confined to two-dimensions of the measurement plane. Three layers of electrodes were used. The current injection was done on the central layer while the voltages were measured from all the three layers. Three individual resistivity distribution images were reconstructed based on the 'method of sensitivity regions' [9]. By subtracting an appropriate proportion of the upper layer and the lower layer from the central layer, the final image was obtained. This resulted in the image having of poor resolution due to the fact that the input current did not travel in a straight-line path, but rather spread all over the phantom under study [10]. The poor resolution of the reconstructed image was also due to the variation of conductivity, σ, in the phantom.

Consider a point 'P' inside a unit circle with cylindrical polar co-ordinates (r, θ) and with conductivity distribution, $\sigma = \sigma(r, \theta)$ as seen in Fig. 2. When σ varies, it is difficult to interpret the current density. However, if σ is a constant i.e. σ is circularly symmetric, $\sigma = \sigma(r)$ which is 'onion –like' then the current lines would travel in straight lines.

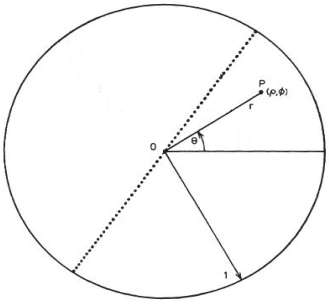

Fig. 2: Coordinate systems. Arbitrary point P has cylindrical polar coordinates (r, Θ) with origin O and curvilinear polar coordinates with origin O; Φ is constant on the curved dashed lines and ρ is constant on the curved full line intersecting the dashed line as redrawn from [11].

In reality, not all practical cases have 'onion-like' conductivity distributions. An analytical method suggested that any reconstruction algorithm that is iterative and can converge, would provide a unique solution for the problem of impedance imaging [11].

Since the development of the first EIT systems, more than three decades ago, researchers have tried their ways to improve the quality of the reconstructed image with regards to the spatial resolution of the final images. Both hardware improvements and software developments have been considered by researchers to improve the quality of reconstructed EIT images as discussed below.

Factors limiting resolution

Hardware

The resolution of the reconstructed images largely depends on the EIT hardware. This includes the operating frequencies, electrodes, the current source and the excitation techniques.

The sensitivity of the EIT systems ranges from approximately 77% to 90%. It was found to have a limited accuracy at higher frequencies. At higher frequencies (more than 100 kHz), the measurement hardware introduces an additional capacitive artifact, possibly caused by the distant location of the current source circuit with respect to the array of electrodes, which alters the impedance measurements. This limits the operating frequency to a maximum frequency of 100 kHz in order to produce decent images [12].

Compound electrodes, which reduce electrode contact impedance, were suggested for better spatial resolution of the reconstructed images. They have large outer current injection electrodes and a small inner voltage measuring electrodes. The smaller areas of the voltage measuring electrodes can sense the voltage at a specified location [13]. However, there are a lot of electric field lines, which gradually decrease when going to the center of the objects in the volume measured. Therefore, the measurements are greatly affected by the objects that are nearer to the electrodes [7]. Hence, the spatial resolution is low, especially in the areas where the current density is low, e.g. near the center of the sensing field. To overcome this problem, an inner-outer sensor structure was proposed. This sensor contains both internal and external electrodes. The internal electrode is the electrode inside the sensing field. The internal electrodes are mounted on the internal structures and have proven helpful for improving the spatial resolution. However, they are fixed in the center of the sensing domain and the number of these internal electrodes are limited.

Under some measurement strategies, the internal and external electrodes work together. A 3D model was used to test the performance of the inner-outer sensor. Six different inner-outer sensor types were designed with different characteristics such as size, number and distribution of the internal electrodes. The 3D reconstruction results showed that the inner-outer sensor have better reconstruction performance than the conventional sensor with only external electrodes [14].

On the other hand, the larger area of current injection electrodes provide uniform current distribution, but there are limits to the inter electrode distance (IED) as shown in Fig. 3.

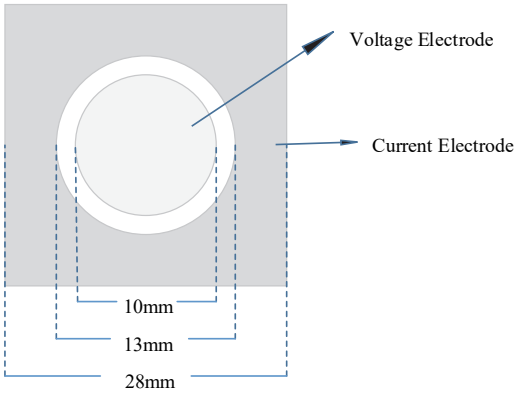

Fig. 3. A compound electrode uses an outer electrode to inject current and an inner electrode to measure voltage as redrawn from [13].

The contact impedance of the voltage electrode does not add to the measured voltage as the current flowing through the voltage electrodes is negligible. Only the current electrodes contribute towards the contact impedance and hence to the measured voltages. For a conventional electrode, the voltage drop in the contact impedance is included in the measured voltage [13].

IED is another factor determining the spatial resolution of the reconstructed image. A divided electrode having two current electrodes on either side of a voltage electrode was developed. Currents were injected into all the current electrodes simultaneously and the voltages were measured from the voltage electrodes differentially. The number of impedance measurements measured at once was the product of the number of current electrodes, m, and the number of voltage electrodes, n, for a total of m×n. Thus high speed and high resolution readings were expected.

However, it was found that the spatial resolution depended on the IED [15].

To achieve better resolution one has to use more electrodes. One can then expect better images by applying a sufficiently high current, which is often not practically safe. Also, if one uses more electrodes but uses only one current source, the resolution would not improve [16]. In general, as more electrodes are used, the contact area of the electrode decreases, which decreases the distinguishability. Hence, one has to apply currents simultaneously to all the electrodes when more of them are used. But this requires as many current sources as the number of electrodes making the circuit more complex and expensive [17]. Even then, the resolution is limited by increasing the number of electrodes. The best EIT image has a resolution of 32×32 pixels with 32 electrodes. By merely increasing the number of electrodes, it will not increase the resolution of the reconstructed image [18].

According to Murphy and York [19], to increase the number of independent observations for EIT, a method of rotation using a mixing impeller is used. Studies show that when the current driving electrodes are attached to the impeller blades, the central sensitivity will be improved and an increased number of independent measuring positions is achieved. The number of independent measurements improve the resolution and information content of EIT reconstruction. The number of odd components of an EIT inversion are steady enough for recovery with an increase in the number of impeller orientations. This lead to more independent learning image content available compared to conventional fixed electrodes. According to the physical data, the amount of recoverable independent image content is approximately four times greater by using the impeller-mounted electrodes. The number of impeller orientations is limited in terms of large data acquisition times and computational complexities.

Similarly, a rotational EIT (REIT) was developed to enhance the quality of the EIT images through more voltage measurements with limited number of electrodes as shown in Fig. 4. Simply increasing the number of electrodes meant expensive hardware and slower data acquisition. The rotating electrodes were used to provide more voltage measurements. The rotations are provided through a stepper motor with step angles as small as 0.018 degree. Compound electrodes were used for the intended study. However, more voltage measurements consumed more processing time making the image reconstruction somewhat difficult. Applying larger currents to the electrodes would also increase the image resolution by reducing the effects of contact impedance, but not for the compound electrodes. In this mechanism, the adjacent method protocol was used to collect the data. This is because by applying this method, 20 independent impedance measurements can be obtained.

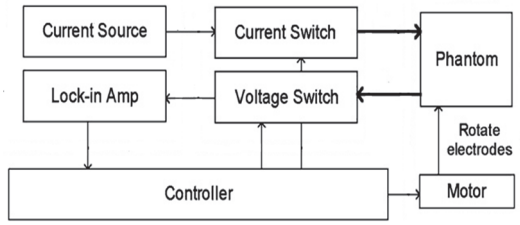

Fig. 4. Block diagram of a REIT system based on [20].

As such, on the next data-acquisition process, there will be 20 more impedance measurements available. When having these additional independent impedances, the reconstructed image undoubtedly could achieve a higher resolution compared to other images produced by the conventional EIT systems [20].

Special electrodes with a limitation of capacitive noise were also designed [21]-[22] to improve the resolution of the images as seen in Fig. 5.

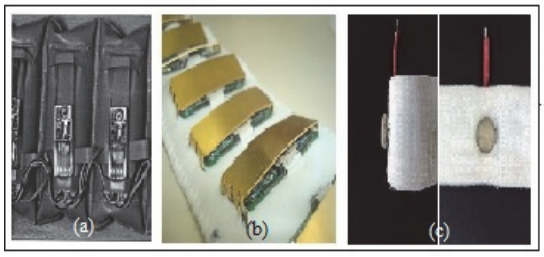

Fig. 5: (a) Inflatable belt [21] (b) Active electrode belt [22] (c) Nano fiber web electrode belt [23].

Gaggero et al. [22] developed an active electrode EIT system in which each active electrode comes with its own signal conditioning circuitry, which reduces the input impedance and hence can contribute towards better resolution of the images. This belt can be used for one time study (Fig. 5(b)). The stray capacitance problems of the cables can be reduced by housing the signal conditioning circuitry close to the active electrodes. Similarly, a flexible belt was designed by Oh et al. [23] using Ag-plated PVDF nano fiber web electrode, but it came with cumbersome wires and larger noise levels even though the contact impedance was observed to be stable.

Poor resolution could be also due to data acquisition electronics limitations, manifest as measurement errors. For example, different excitation techniques and measurement methods affect the signal-to-noise ratio (SNR) of the measured data. To address this Isaacson [24] suggested a measurement method for the best distinguishability. If 'r' is the resistance matrix with an actual resistivity distribution and 'ř' is for measured resistivity distribution, the voltage difference 'Δv' for a given current 'i' is, Δv=(r-ř) i. Here, 'Δv' is important for the estimation of the resistance. The diagonal method of current injection produced better quality images when compared with the neighboring method, but it comes

with some measurement errors. The Fourier based method, however, shows smaller measurement errors and hence is considered the most accurate method of current injection (not suitable for biological studies) [25].

Tafiei-Naeini and McCann [26] suggested better resolution with multiple current sources at the expense of EIT hardware. Their proposed system was not only complex but also required balanced output impedance and phase among the current sources. The SNR of the excitation current source also added to the spatial resolution of the EIT systems. A current sub-system was designed to provide an SNR of 80 dB.

Excitation methods and voltage measurements also contribute towards the resolution of the EIT images. For a single current source, an adjacent current pattern can detect objects whose size are greater than a fist within the confines of chest sized test tank. For the opposite current pattern, objects whose size is greater than two fingers could be detected, and one cosine pattern was observed to detect with the resolution of a finger's width [10].

In general, for better readings and hence for better resolution, the measured voltages should account for only the resistance and the real component as its the impedance, but not the imaginary component as its parasitic capacitances give rise to measurement errors [27].

Furthermore, detectability (sensitivity) is influenced by the current injection methods (Fig. 6) whereas distinguishability (spatial resolution) is influenced by the voltage measurement technique.

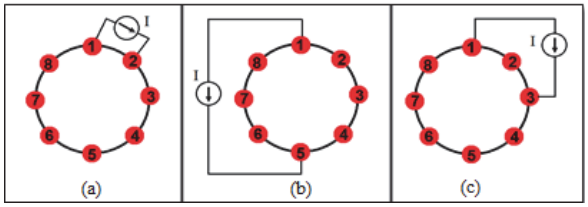

Fig. 6: (a) Neighboring (b) Opposite (c) Cross methods of current injection.

The resolution of the reconstructed images is at its worse at the center of the test object because it is always not practical to place the electrodes inside. Two layers of 16 electrodes were considered. Both the adjacent and opposite current injection methods were employed. The voltages were then measured horizontally adjacent, vertically adjacent, and for all possible adjacent combinations.

A full width half maximum (FWHM) method was then used to analyze spatial resolution. It gives the distances between the two points of an image sharing the same solution value, which is half of the peak value. The lesser the FWHM percentage, the higher will be the spatial resolution. The use of two layers provides somewhat better information about the test object [28].

One other reason for low resolution is that the measurement sensitivity decreases drastically with the increasing distance from the electrodes. Ts et al. [29] proposed an EIT system with a novel electrode configuration to address this limitation. In this system, two pairs of driving electrodes attached on four sides of the surface of the body, and an array of voltage sensing electrodes are placed along the surface as shown in Fig. 7.

As the current injection and voltage sensing electrodes are separated, no current actually flows through the voltage sensing electrodes given their contact impedance. The current injected flows underneath the voltage sensing electrodes, allowing the voltage to be measured in the normal direction to the voltage sensing electrode array. However, blur images are unavoidable when using this electrode configuration when the distance from the object surface is too large. Therefore, a process known as de-blurring was suggested to improve the spatial resolution of images.

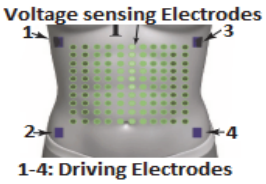

Fig. 7: Novel electrode configuration based on [30].

One such method, a layer stripping method, was proposed by Somersalo [30] that focused on providing good reconstruction near the boundary. In this method, current with rapid spatial variation is supplied to the surface so that the current does not penetrate deeply into the body or object. As such, the difference in boundary voltage will be affected mainly due to the impedance change near the surface. Provided there is only a small error in the measurement, a high-resolution image may be obtained in the region near the surface. In the applied potential tomography systems, a voltmeter having high input impedance must be used for measuring the voltages to avoid the pitfalls of electrode contact impedance. Moreover, the voltages of the current receiving electrodes are neglected for the same reason. Further, the measured voltages are added up to improve the SNR improving the resolution of the reconstructed images [11].

Hence, spatial resolution of EIT depends on several hardware factors, which include the noise of the measurements, the number of electrodes, the current excitation methods, and voltage measurement techniques used.

As such, the spatial resolution of the image reconstructed varies from one device to another. Different methods and models have been proposed to overcome this limitation, however in practicality, it is still difficult to

achieve high quality images from any EIT systems without the state-of-the-art electronic instrumentation.

Imaging Techniques

Several reconstruction algorithms have been developed for the reconstruction of the EIT images focusing on the improvement of the reconstructed image resolution.

Based on the type of imaging, there are two types of techniques that can be approached in EIT systems, dynamic imaging and static imaging. In dynamic imaging (with a focus on temporal resolution), boundary voltages are measured at different time intervals, and the first data at initial time (t_1) is treated as the reference data set for another data set measured at a second time (t_2). By back projecting the difference an image is reconstructed [31]. In static images (spatial resolution), the absolute values of a cross-sectional resistivity distribution are reconstructed from voltage measurements, which is a function of an unknown resistivity distribution. This makes the image of reconstruction a nonlinear problem. The Newton-Raphson method, demonstrated by Yorkey et al. [32] produced good quality static images provided there was no error in the modeling and measurement of the voltages (or, current). When errors are present and the number of elements increased to get a good spatial resolution, the images distort greatly. Isaacson [24] and Gisser et al. [33] proposed an optimized current injection method which injects a certain pattern of current through the electrodes. This novel method of current injection combined with the Newton-Raphson method yields a good static image. An EIT system that uses 32 electrodes of 12-bit resolution with optimal current injection was developed as shown in Fig. 8.

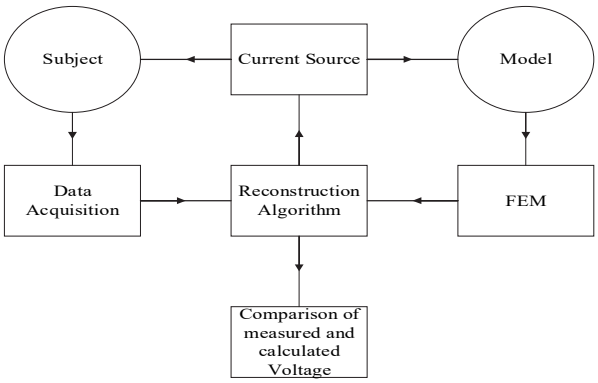

Fig. 8: Block diagram of the EIT system redrawn from [31].

A specially designed digital voltmeter was used to acquire the boundary voltages from the electrodes. The measured voltages were compared to the computer model voltages and depending on the difference in reading (error) the computer model voltages were adjusted accordingly. The computer model voltages were calculated using a finite element method to develop the voltages with an assumed model resistivity distribution since the problem is nonlinear [34]. Reconstruction was done based on the model described by:

$$Min_{\rho} Max_{c,e} \varphi(\rho; c; e) \quad (1)$$

where, $\varphi(\rho; c; e)$ is an objective function (error), ρ is resistivity distribution of model, c is the injection current pattern, and e is the electrode configuration. In this case, the algorithm was assumed correct but the unknowns of the model must be found.

To make the EIT system more efficient, requires a measurement method (comprising current injection patterns, electrode size, position, etc.), which ultimately maximizes the objective function/distinguishability. An algorithm is needed to adjust the distribution of resistivity. It is required to solve the forward problem for equation (1). A forward problem is needed to compute boundary voltages of a subject with a given resistivity distribution in response to an injected current. This can often be challenging, as most samples under examination are nonhomogeneous, anisotropic, and irregularly shaped. Therefore, approaches taken to solve the forward problem often employ numerical methods and more specifically, finite element methods.

A circular finite element method for EIT was developed by Woo et al. [35]. They describe a sparse matrix method for solving the forward problem and for reconstructing the static EIT image, going so far as to create a finite element software package, which included finite element mesh generators, efficient sparse matrix, and vector algorithms for solving sparse linear system of equation.

The distinguishability, d, of an injection pattern, c, is the ability to distinguish two different resistivity distributions [24]. The equation below shows how distinguishability can be calculated:

$$d = \left| \frac{v_1 + v_2}{c} \right| \quad (2)$$

where v_1 and v_2 are the boundary voltages due to distribution of resistances Ω_1 and Ω_2 respectively.

This part solves the Max part of equation (1). To get a good static image, the electrodes were placed equally and the injected current pattern used was developed using the Walsh function [36].

Many EIT images are generated based on the distribution of conductivity changes within the volume. In this scenario, the most ideal case to arrive at the conductivity distribution via an inverse solution is to know the voltage along the whole surface of the volume's boundary; however, this is often not possible since the voltage measurement of the surface is restricted by the signal-to-noise ratio. This makes it hard for the reconstruction algorithms to come up with the conductivity distribution. To compensate for such limitations, two approaches are employed: linear

approximations and non-linear approximations. Non-linear approximations tend to produce better images but requires more computation time, while conversely, linear approximations tend to use less computation time and produce images with low spatial resolution. The most common linear inverse solvers are – generalized vector sampled pattern matching (GVSPM), a pseudo-invasive method, and the standardized low resolution electromagnetic tomography algorithm (sLORETA) [37].

An algorithm that uses a linear approximation solver to produce an image with better spatial resolution was presented. This was done by using a focal underdetermined system solver (FOCUSS) algorithm which is an initialization-dependent recursive algorithm that produces solutions based on a weighted minimum-norm least-squares solution [38]. In short, it takes a low spatial image and employs a re-weight strategy that improves the spatial resolution during its iterations [39]. The linear inverse solver used in this experiment was sLORETA and the FOCUSS was used in the re-weighting. Furthermore, a shrinking strategy was used to reduce the processing time. The combination of the shrinking strategy and FOCUSS is called shrinking-FOCUSS. The developed algorithm is called shrinking sLORETA-FOCUSS. The algorithm was tested on a realistic 3D head model around which electrodes were placed. Before the algorithmic implementation, the EIT forward problem was solved with a model of known conductivity distribution subjected to low frequency current. A large number of electrodes were connected and thus a shrinkage method was used to reduce the solution space and a weighing matrix made the process take less time since this included less elements for the algorithm to handle during iteration [37].

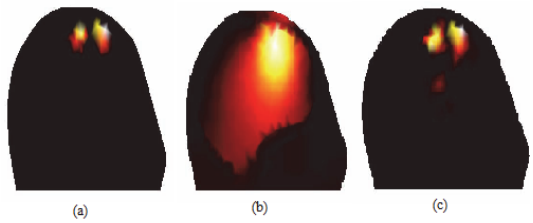

Fig. 9: Longitudinal section of the reconstructed images with the perturbations located in the movement region of the brain a) The original distributions of the two perturbations (b) The images reconstructed by the sLORETA alone (c) The images reconstructed by shrinking sLORETA-FOCUSS based on [37].

In this experiment, a 3D realistic head was used and 32 electrodes were placed around it. The electrode placement was done based on 10-20 EEG electrodes system. An injection protocol was made with the aim of maximizing sensitivity to impedance changes and as such a current was injected to the opposite electrodes and the neighboring electrodes were used for measuring the voltages. A total of 258 voltages were taken for each image. The last part of the experiment involved simulation of the image using different algorithms like perturbations and sLORETA. The final image was simulated using the shrinking sLORETA-FOCUSS. The results of the experiment are shown in Fig. 9 illustrate the effects of different algorithms. It can be seen that the shrinking sLORETA-FOCUSS method produced images with good spatial resolution and the shrinking strategy increased computation efficiency greatly. Indeed, the only shortfall of this algorithm appears to be that it has not been researched in greater detail. For example, it has not yet been used on live tissue or on human subjects, and thus its performance in real world situations is not clear. In short this algorithm shows great potential in 3D image reconstruction with good spatial resolution, but warrants further investigation [37].

EIT algorithms may also be categorized as iterative algorithms and direct algorithms. The former tends to yield better results but utilizing more computation time, while, the latter gives less accurate results provided as faster solutions [40].

Mueller et al. [41] focuses on the direct image reconstruction with applicability to the medical field. The direct image reconstruction allows for the rapid generation of a series of images, thereby making it possible to monitor living tissues. Their work proposes a mathematical algorithm based on a proof of the 2D-inverse condition problem [42]. The algorithm, tested on a chest model, determines the scattering transform, t, from a Dirichlet-to-Neumann map from which it reconstructs the conductivity distribution. The experiment was designed using a virtual chest phantom. This virtual chest was constructed using elliptical domains to represent the heart and lungs. The resistivity of the models representing the heart and the lungs was selected based on the behavior that an organ with more blood has a lower resistivity compared to an organ with less blood. The resistivity of these organs also changes during different physiological states, e.g., the resistivity of the heart increases during systole while the resistivity of the lung decreases during exhalation. The background conductivity was set to a constant value of conductivity of 1. Polynomial smoothing was applied in smoothening the edges of the organs during reconstruction since the method is only valid for conductivities with two derivatives. The reconstructed images are shown in Fig. 10. The images were reconstructed from the conductivity of the model chest.

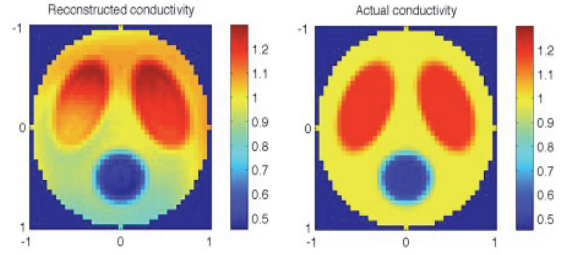

Fig. 10: Plots of the actual and reconstructed conductivities for the virtual phantom chest as re-arranged from [41].

Polydoride and McCann [43], implemented an algorithm based on Newton's iterative techniques for nonlinear image reconstruction. This method integrated a linear regularized step based on the regularized total least square (RTLS) problem. Although the formula is same as the Tikhonov problem, the RTLS differs when the inverse problem is solved under the assumption, that both measurement and the sensitivity values are known roughly. The RTLS problem can formulated in the same way as the Tikhonov problem, which includes one additional factor and requires an estimation of two scalar parameters. The Jacobian method is another approach wherein the inverse solution can be calculated with a coarser model (in this case with 816 elements). This is due to the use of a different finite model for the forward and the inverse problem, which largely reflects the perfected model. The noise is added to perfect the instrumentation noise, which pollutes the measurement when doing data acquisition. A system with 22 electrodes was employed to perform spatial resolution comparison with the conventional scheme. After applying the 11 opposite current patterns, 198 stimulated measurements were collected. The images for the spatial resolution were obtained by calculating the normalised spatial resolution error.

The modified Newton-Raphson algorithm offers good spatial resolution for static objects operating under the assumption that no significant measurement noise is present. However, practical applications are susceptible to various sources of noises [24]. An open EIT model using the Newton-Raphson algorithm was also developed with Tikhonov regularization. Good resolution was achieved, but the method was unsuitable for test objects lying on the extremes [44]. The same regularization method was optimized for better accuracy by Aristovich et al [45].

A major way of improving spatial resolution is by filtering or correcting the data acquired by the electrodes. This approach may improve the spatial resolution greatly without requiring improved hardware. According to Holder [46], a standard method of altering the error reading is by using a regularization technique called Tikhonov regularization. This method uses a suitable regularization parameter on the matrix of the data acquired. This method smooth the results, and truncates the errors in a linear way. However, the system is nonlinear, such that this method only improves spatial resolution to a certain point past which further application can distort the results.

Another technique proposed by Tushar et al. [47] to improve the spatial resolution of EIT reconstruction images is projection error propagation – based regularization (PEPR). The PEPR method defines the regularization parameter as one of the functions of the projection error, which is caused by a difference between experimental measurements and calculated data. This indicates that the magnitude of the regularization parameter actually varies according to the projection error. For a larger projection error, a greater regularization value needs to be set to regulate the process during iterations. In addition, the regularization parameter in the image reconstruction algorithm will be modified automatically according to the noise level in the measured data. Therefore, even with noisy boundary data, the PEPR method is able to produce improved reconstruction images with high contrast.

Based on the spatial resolution result of EIT, Yan et al. [48] used the coercive equipotential node model, taking the widths of the excitation electrode and the measurement electrode into consideration. The simulation platform, based in Visual C++, defines the estimation image reconstruction quality and measurement sensitivity to create a simulation to study EIT electrode structure and parameter impacts. The influences of line electrode and compound electrode were studied. By using the simulation result, an optimized design for the electrode structure and its parameter was found. For the line electrode, even though it is a wider electrode that can reduce the contact impedance between the electrode and skin, the simulation result proved that increasing the width of a line electrode width increase not necessarily increase performance. For instance, using too wide of a line electrode can reduce measurement sensitivity. To overcome this, an optimal measurement sensitivity was found for different widths of the line electrode at different measurement depths. The application object in this EIT is often an area with a circular boundary. Thus, when the boundary size and electrode number is determined, the sum of the electrode width and the distance will be fixed. It is reasonable to assume using a wider electrode will reduce the electrode distance. Furthermore, it would be difficult to image deep into the centre of the measured field if the electrode distance is too short under the measurement current of EIT. Hence, the measurement sensitivity will be affected by depth especially towards the centre area. For the compound electrode, increasing the distance between two adjacent compound electrodes can advance the reconstructed image quality of the centre area. This lowers the reconstructed image quality of the superficial layer of the area in favour of improved uniformity of the reconstructed image quality over the whole measured area. The compound electrode has a complex structure, which includes complex structure parameters. Due to the circular boundary, the parameters are limited to each other and mutual influences are more difficult. The impacts of all parameters should be considered carefully, especially the distance between two adjacent compound electrodes and their width.

Image fusion techniques are one of the current research topics of interest for enhancing EIT image quality. An image fusion algorithm based on wavelet-transform was reported by Li et al. [49]. Two images from different algorithms (one from a singular value decomposition (SVD) algorithm and

other from a conjugate gradient (CG) algorithm [50]) were fused using the proposed technique. The image formed by this algorithm was essentially a combination of two images, which had been reconstructed separately by the SVD and the CG methods. The process of reconstructing the image using the algorithm proposed was formed by initially taking measurements of the ERT system and later using this data to form two images by the SVD and CG method. The images were then decomposed by wavelet transformation and then used to construct a wavelet pyramid separately. The two images that have been decomposed and fused separately have different frequencies. The different frequency components on the decomposed layer apply different fusion operators. The wavelet pyramid was then obtained. The final image that was reconstructed is obtained by inverse discrete wavelet transformation of the wavelet pyramid. The reconstruction algorithm was programmed in MATLAB 7.1 and COMSOL. The image obtained from image fusion algorithm were compared to images obtained by the CG and SVD methods independently. The comparison was based on the relative error of image reconstruction [51]. The image fusion method was found to produce smaller errors compared to the CG and SVD methods independently in all the situations and different images that were tested. Even though the errors in the images formed by CG and SVD methods changed depending on the situation, the SVD approach was better in one situation while CG was better in another. The main challenge with the image fusion algorithm was that it required more processing time to reconstruct one image; for that image to be formed, it was required to reconstruct two images using the different methods and then to combining them using the proposed algorithm. With sufficient processing power, this approach could work best since, in theory, combining more images from different algorithms would result in better spatial resolution image [49].

Davidson et al. [52] demonstrated a scanning technique that offered good spatial resolution at the same time and provided continuous image generation to monitor patients using a technique to fuse EIT images with the corresponding magnetic resonance imaging (MRI) images. The first step was to convert the EIT image into a matrix with 2 mm^3 isotropic voxels by using a software package known as Manchester Confeitir [53]. The MRI and EIT images were then fused together using an open-source software called 3D-Slicer. The images were overlaid and aligned manually. The algorithm developed during the experiment can be seen in Fig. 11 and shows that using this image to monitor any vital organ or area of interest is possible since the MRI image provides good spatial resolution while the EIT image shows the activity taking place continuously. This technique can only be implemented with the aid of an MRI imaging machine [52].

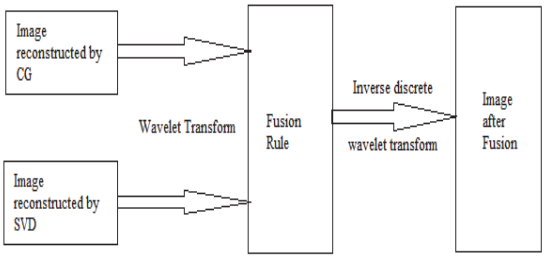

Fig. 11: Wavelet image fusion algorithm redrawn from [52].

Similarly, Chen et al. [54] presented an approach to improve spatial resolution by partly solving the forward problem of EIT, given physical and structural information about the test sample. The algorithm used in this experiment was a conjugate gradient (CG) algorithm. The approach proposed in this paper was carried out on an EIT system that consisted of 16 electrodes, a signal generator, that was to deliver sinusoidal current and 2-to-16 multiplexer was used during current injection. The function generator injected current with a frequency ranging from 10Hz to 500 kHz. The sensitivity of the electrodes at the boundary was improved by incorporating the boundary and physiological stricter. This was the information of the human thorax taken from CT scan. The image from the CT scan was divided into segments, which consisted of segments of different organs like the heart, lungs, spinal column, and skeletal muscle. The segmented sample is shown in Fig. 12.

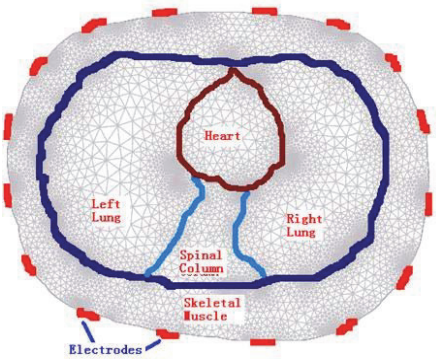

Fig. 12: Meshes refined by COMSOL based on [54].

These boundary conditions were fed into the mathematical model and the conjugate gradient least square (CGLS) algorithm, which is an improved version of the CG algorithm that was used in the reconstruction. A differential imaging strategy was used with the aim of reducing instrumentation and modeling errors. The results are shown in Fig. 13.

EIT images were taken with air in the lungs and without air in the lungs. In this case, the EIT images showed that the left lung was smaller than the right lung, a result consistent with those of the contemporaneous CT scan.

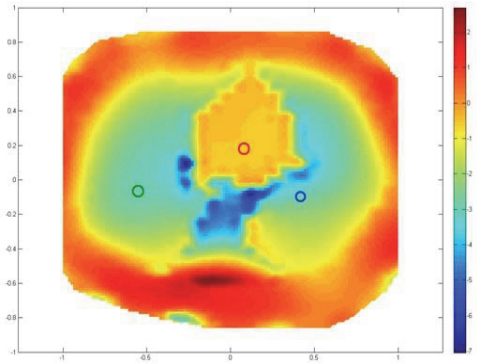

Fig. 13: Locations of 3 representative pixels in grids based on [54].

The main challenge with the approach from Chen et al. is that to address the forward problem, a CT scan is required. This means that this method can only be used for monitoring since for it to be effective there must be an original image from CT [54]. Therefore, a priori information of the test object is required for the fusion techniques. Usually a technique with good spatial information (such as MRI, CT), etc., is fused with a technique like EIT with good temporal information [55].

Olmi et al. [56] introduced another reconstruction method, called genetic algorithm EIT (GA-EIT). The first part of this reconstruction deals with the underlying mathematical principles, which will not be covered here since they delve more deeply into the double-constraint (DC) and Newton-Raphson (NR) methods. For the reconstruction to be accurate, it is assumed that no current escapes the test sample and the resistivity distribution is derived from boundary voltages, which are a result of injected current. In implementing the GA-EIT, a number of images that is referred to as a set or population is generated. A fitness value is assigned to each element of conductivity. The fitness values are then ranked based on the quality or correctness of the image. The fitness value with a good image are given a better ranking or a better chance for them to contribute to the successive generation and mutation. A termination criterion is applied after this stage. The termination is done when convergence has been reached or if the maximum number of generation has been exceeded. When the convergence has not occurred, the process is repeated for the selected population or otherwise the fittest individuals are considered the solution of EIT problem. The genetic algorithm process was modified as it was implemented in the experiment. To reduce the time taken, three stages were followed to generate the population. These steps eliminate the random generation of population. The first two stages supply useful genetic material to the target population and this reduces the time to get an accurate solution. The GA-EIT implementation uses a fixed sized overlapping population and hence GA-EIT provides its own constraints. GA-EIT images were compared to those generated by a modified NR method [32] and a DC method [57]. In both cases, the GA-EIT used 16 and 32 individuals. The DC image was inferior when compared to the GA-EIT image. With 32 individuals, GA-EIT produced a good image but took longer to reconstruct the image. GA-EIT image that used 32 individuals looked better than the NR image, but the NR method produced a better image compared to that of the DC method. The GA-EIT approach in reconstruction is computationally expensive in the sense that it requires and a good processor to compute. The GA-EIT approach, due this limitation, is now being used in static image reconstruction only.

In summary, the best way to improve the spatial resolution of EIT is to select a good algorithm to regularize the data, and another good algorithm to reconstruct the image from the data.

EIDORS is an open source software for EIT applications, which can be used as a reference software for the newly developed algorithms of EIT systems. It uses a finite element model to formulate the forward problem and regularization techniques to solve the inverse problems. The EIDORS environment comprises four main blocks: forward model, data, inverse model, and image.

The forward model formulates the forward problem of the EIT systems by defining the input currents and electrode specifications based on the finite element method. The data refers to the measured voltages or the simulated voltages. The inverse model gathers all the necessary information from the forward model and the data. Finally, the data is reconstructed in the form of an image.

Although EIDORS has been accepted by many researchers for its inverse problem solving, it currently experiences problems when dealing with a large set of data. It has been observed that there are interactions among the different parts of the algorithms when handling large data, which results in the misinterpretation of the results. In addition, care must be taken during the noise selection and during the assumption of the inputs and variables. Model errors are also visible, but this cannot currently be addressed in the EIDORS software [58].

Further Possible Improvements

Based on a review on the literature, it can be seen many factors contributing to the spatial resolution of EIT images. A new approach toward enhancing spatial resolution is an array processing technique. The purpose of this proposal is to overcome the problem that arises upon image reconstruction, which is sacrificing computational efficiency and time for better image accuracy or sacrificing image accuracy for a quicker and efficient processing time. The proposed algorithm provide a balance, producing more accurate results more efficiently. It can provide a better image of accuracy or resolution in the shortest time possible.

An array processing technique uses an array of similar sensors that are spatially separated to analyze the area in between (this includes signals such as those from radar,

sonar, radio astronomy, satellite communications, direction finding, seismology, tomography, etc. [59]). Array processing techniques have been used previously in medical applications includes ultrasonic imaging for fetal development monitoring and observation of the blood flow in the heart valves [60] and EEG signal processing for neurological disorders [61]. Both of these applications use the concept of beamforming [62], which estimates a signal from a specific sensor in a desired direction and separates signals from the remaining sensors from other directions. A major advantage of the beamforming technique is its spatial discrimination of the signals with an array of sensors [63].

Wideband beamformers have been previously used for medical diagnosis. An ultra-wide band beamformer was used to detect early breast tumors using microwave technology. If for the presence of a tumor, the beamformer output shows a large energy signal. Thus, the signal as a function of location provides an image. However, neither the shape nor the size of the tumor is known, and further analysis is required [64]. Cao and Nehorai [65] used a delay-and-sum beamforming algorithm to reconstruct an image of the breast. Peak-to-peak value indicates abnormality in the breast. Tumor localization was done using optical tomography and beamforming. This method was effective in improving the spatial resolution up to 1.5 cm and above. However, the resolution was affected by an increase in the noise levels [66]. The beamforming technique was also proposed to study the temporal changes. Prior computed tomographic images were used as a reference set for the study [67]. The beamforming technique can be introduced to the EIT systems in order to study conductivity changes. In spite of simpler computations, the noise effect was a major drawback in this system [7].

Conclusion

An extensive review on the spatial resolution of the electrical impedance tomography systems is covered in this paper. Hardware improvements and software developments are highlighted. An array processing technique could be the possible new dimension towards the improvement of spatial resolution for the future EIT applications.

References

1. A. C. Kak and Malcolm Slaney, Principles of Computerized Tomographic Imaging. IEEE Press, 1988.
2. M. S. Williams, R.A. Beck, Process Tomography. Elsevier, 1995.
3. R. Leroy, "April 1979," Weatherwise, vol. 32, no. 3, pp. 135–138, 1979. https://doi.org/10.1080/00431672.1979.9930084
4. G. J. Saulnier, R. S. Blue, J. C. Newell, D. Isaacson, and P. M. Edic, "Electrical impedance tomography," IEEE Signal Process. Mag., vol. 18, no. 6, pp. 31–43, 2001. https://doi.org/10.1109/79.962276
5. K. R. Spring, "Spatial Resolution in Digital Images," 2016. [Online]. Available: http://micro.magnet.fsu.edu.
6. B. Sun, S. Yue, Z. Cui, and H. Wang, "A new linear back projection algorithm to electrical tomography based on measuring data decomposition," Meas. Sci. Technol., vol. 26, no. 12, p. 125402, 2015. https://doi.org/10.1088/0957-0233/26/12/125402
7. J. S. Lioumbas, a Chatzidafni, and T. D. Karapantsios, "Spatial considerations on electrical resistance tomography measurements," Meas. Sci. Technol., vol. 25, no. 5, p. 055303 (12 pp.), 2014. https://doi.org/10.1088/0957-0233/25/5/055303
8. R. P. Henderson and J. G. Webster, "An impedance camera for spatially specific measurements of the thorax.," IEEE Trans. Biomed. Eng., vol. 25, no. 3, pp. 250–254, 1978. https://doi.org/10.1109/TBME.1978.326329
9. P. M. R. and P. R. R. Gadd, F. Vinther, "Reconstruction of 3D data for Electrical Impedance Tomography," Electron. Lett., vol. 28, no. 11, pp. 974–976, 1992. https://doi.org/10.1049/el:19920619
10. C. C. Barber, B. H. Brown, and I. L. Freeston, "Imaging spatial distributions of resistivity using applied potential tomography," Electron. Lett., vol. 19, no. 22, p. 933, 1983. https://doi.org/10.1049/el:19830637
11. A. D. Bates, R. H. T. Mckinnon, G.C. Seagar, "A Limitation on Systems for Imaging Electrical Conductivity Distributions," IEEE Trans. Biomed. Eng., vol. 27, no. 7, pp. 418–420, 1980. https://doi.org/10.1109/TBME.1980.326657
12. M. S. Campisi, C. Barbre, A. Chola, G. Cunningham, V. Woods, and J. Viventi, "Breast cancer detection using high-density flexible electrode arrays and electrical impedance tomography," 36th Annu. Int. Conf. IEEE Eng. Med. Biol. Soc., pp. 1131–1134, 2014. https://doi.org/10.1109/embc.2014.6943794
13. P. Hua, E. J. Woo, J. G. Webster, and W. J. Tompkins, "Using compound electrodes in electrical impedance tomography.," IEEE Trans. Biomed. Eng., vol. 40, no. 1, pp. 29–34, 1993. https://doi.org/10.1109/10.204768
14. R. Shangjie, T. Chao, X. Yanbin, and D. Feng, "Performance Evaluation and Structure Optimization of an Inner-outer Electrical Resistance Tomography Sensor," vol. 1, no. ICMC, pp. 1–5, 2014. https://doi.org/10.1109/icmc.2014.7231819
15. Morimoto, E. Yasuno, Y. Kinouchi, Y. Ohmine, a Tangoku, and T. Morimoto, "Spatial resolution in the electrical impedance tomography for the local tissue.," Annu. Int. Conf. IEEE Eng. Med. Biol. Soc., vol. 6, pp. 6638–41, 2005.
16. J. C. Gisser, D.G. Isaacson, D. Newell, "Electric current computed tomography and eigenvalues," SIAM J. Appl. Math., vol. 50, no. 6, pp. 1623–1634, 1990. https://doi.org/10.1137/0150096
17. E. J. D. Bronzino, "Electrical Impedance Tomography," Biomed. Eng. Handb., vol. 41, no. 1, pp. 85–101, 2000.
18. I. Frerichs, J. Scholz, and N. Weiler, "Electrical Impedance Tomography and its Perspectives in Intensive Care Medicine," Yearb. Intensive Care Emerg. Med., pp. 437–447, 2006.
19. S. C. Murphy and T. A. York, "Electrical impedance tomography with non-stationary electrodes," Meas. Sci. Technol., vol. 17, no. 11, pp. 3042–3052, Nov. 2006. https://doi.org/10.1088/0957-0233/17/11/025

20. C.-N. Huang, F.-M. Yu, and H.-Y. Chung, "Rotational electrical impedance tomography," Meas. Sci. Technol., vol. 18, no. 9, pp. 2958–2966, 2007. https://doi.org/10.1088/0957-0233/18/9/028
21. R. J. Sadleir, R. A. Fox, and V. F. Turner, "Inflatable belt for the application of electrode arrays," Rev. Sci. Instrum., vol. 71, no. 2, pp. 530–535, 2000. https://doi.org/10.1063/1.1150236
22. P. O. Gaggero, A. Adler, J. Brunner, and P. Seitz, "Electrical impedance tomography system based on active electrodes," Physiol. Meas., vol. 33, no. 5, pp. 831–847, 2012. https://doi.org/10.1088/0967-3334/33/5/831
23. T. I. Oh, T. E. Kim, S. Yoon, K. J. Kim, E. J. Woo, and R. J. Sadleir, "Flexible electrode belt for EIT using nanofiber web dry electrodes," Physiol. Meas., vol. 33, no. 10, pp. 1603–1616, 2012. https://doi.org/10.1088/0967-3334/33/10/1603
24. D. Isaacson, "Distinguishability of conductivities by electric current computed tomography," IEEE Trans. Med. Imaging, vol. 5, no. 2, pp. 91–95, 1986. https://doi.org/10.1109/TMI.1986.4307752
25. P. Hua, E. J. Woo, J. G. Webster, and W. J. Tompkins, "Improved methods to determine optimal currents in electricalimpedance tomography," IEEE Trans. Med. Imaging, vol. 11, no. 4, pp. 488–495, 1992. https://doi.org/10.1109/42.192684
26. M. Rafiei-Naeini and H. McCann, "Low-noise current excitation sub-system for medical EIT.," Physiol. Meas., vol. 29, no. 6, pp. S173–84, Jun. 2008. https://doi.org/10.1088/0967-3334/29/6/S15
27. B. H. Brown, "Electrical impedance tomography (EIT) a review," J. Med. Eng. Technol., vol. 27, no. 3, pp. 97–108, 2003. https://doi.org/10.1080/0309190021000059687
28. R. K. Y. Chin and T. A. York, "Improving spatial resolution for EIT reconstructed images through measurement strategies," IEEE ICSIPA 2013 - IEEE Int. Conf. Signal Image Process. Appl., pp. 5–10, 2013. https://doi.org/10.1109/icsipa.2013.6707968
29. M.-E. Ts, E. Lee, J. K. Seo, B. Harrach, and S. Kim, "Projective Electrical Impedance Reconstruction with Two Measurements," SIAM J. Appl. Math., vol. 73, no. 4, pp. 1659–1675, 2013. https://doi.org/10.1137/120879671
30. E. Somersalo, M. Cheney, D. Isaacson, and E. Isaacson, "Layer stripping: a direct numerical method for impedance imaging," Inverse Probl., vol. 7, no. 6, pp. 899–926, Dec. 1991. https://doi.org/10.1088/0266-5611/7/6/011
31. D. C. Barber and B. H. Brown, "Applied potential tomography.," J. Br. Interplanet. Soc., vol. 42, no. 7, pp. 391–393, 1989.
32. T. J. Yorkey, J. G. Webster, and W. J. Tompkins, "Comparing Reconstruction Algorithms for Electrical Impedance Tomography," IEEE Trans. Biomed. Eng., vol. BME-34, no. 11, pp. 843–852, 1987. https://doi.org/10.1109/TBME.1987.326032
33. T. G. Gisser, D. Isaacson, and J. C. Newell, "Current topics in impedance imaging," Clin. Phys. Physiol. Meas., vol. 8, pp. 39–46, 1987. https://doi.org/10.1088/0143-0815/8/4A/005
34. E. J. Woo, P. Hua, J. G. Webster, and W. J. Tompkins, "A robust image reconstruction algorithm and its parallel implementation in electrical impedance tomography," Med. Imaging, IEEE Trans., vol. 12, no. 2, pp. 137–146, 1993.
35. E. J. Woo, P. Hua, W. J. Tompkins, and J. G. Webster, "A finite element model with node renumbering for adaptive impedance imaging," Proc. IEEE EMBC, vol.1, pp. 277–278, 1988. https://doi.org/10.1109/iembs.1988.94515
36. R. Pallàs-Areny, J. G. Webster, and W. J. Tompkins, "Using walsh functions in electrical impedance tomography," 12th Annu. Int. Conf. IEEE EMBS, vol. 12, no. 1, pp. 124–125, 1990.
37. G. Dong, R. Bayford, H. Liu, Y. Zhou, and W. Yan, "EIT images with improved spatial resolution using a realistic head model.," Conf. Proc. IEEE Eng. Med. Biol. Soc., vol. 1, pp. 1134–7, 2006. https://doi.org/10.1109/IEMBS.2006.259794
38. F. Gorodnitsky and B. D. Rao, "Sparse signal reconstruction from limited data using FOCUSS: A re-weighted minimum norm algorithm," IEEE Trans. Signal Process., vol. 45, no. 3, pp. 600–616, 1997. https://doi.org/10.1109/78.558475
39. H. Liu, X. Gao, P. H. Schimpf, F. Yang, and S. Gao, "A recursive algorithm for the three-dimensional imaging of brain electric activity: Shrinking LORETA-FOCUSS.," IEEE Trans. Biomed. Eng., vol. 51, no. 10, pp. 1794–1802, 2004. https://doi.org/10.1109/TBME.2004.831537
40. D. C. Barber, "A review of image reconstruction techniques for electrical impedance tomography," Med. Phys., vol. 16, no. 2, p. 162, 1989. https://doi.org/10.1118/1.596368
41. L. Mueller, S. Siltanen, and D. Isaacson, "A direct reconstruction algorithm for electrical impedance tomography," IEEE Trans. Med. Imaging, vol. 21, no. 6, pp. 555–559, 2002. https://doi.org/10.1109/TMI.2002.800574
42. A. I. Nachman, "Global uniqueness for a two-dimensional inverse boundary value problem," Ann. Math., vol. 143, pp. 71–96, 1996. https://doi.org/10.2307/2118653
43. N. Polydorides and H. McCann, "Electrode configurations for improved spatial resolution in electrical impedance tomography," Meas. Sci. Technol., vol. 13, no. 12, pp. 1862–1870, Dec. 2002. https://doi.org/10.1088/0957-0233/13/12/309
44. C.-H. Zhang, Xiao-Ju. Chen, Min-You He, Wei He, "Modeling and simulation of open electrical impedance tomography," Int. J. Appl. Electromagn. Mech., vol. 33, no. 1,2, pp. 713–720, 2010.
45. Y. Aristovich, G. S. dos Santos, B. C. Packham, and D. S. Holder, "A method for reconstructing tomographic images of evoked neural activity with electrical impedance tomography using intracranial planar arrays.," Physiol. Meas., vol. 35, no. 6, pp. 1095–109, Jun. 2014. https://doi.org/10.1088/0967-3334/35/6/1095
46. D. S. Holder, Electrical Impedance Tomography: Methods, History and Applications. Taylor & Francis, 2004. https://doi.org/10.1201/9781420034462
47. T. K. Bera, S. K. Biswas, K. Rajan, and J. Nagaraju, "Improving image quality in Electrical Impedance Tomography (EIT) using Projection Error Propagation-based Regularization (PEPR) technique A simulation study," J. Electr. Bioimpedance, vol. 2, no. 1, pp. 2–12, 2011. https://doi.org/10.5617/jeb.158
48. W. Yan, S. Hong, and R. Chaoshi, "Optimum design of electrode structure and parameters in electrical impedance tomography.," Physiol. Meas., vol. 27, no. 3, pp. 291–306, Mar. 2006. https://doi.org/10.1088/0967-3334/27/3/007

49. S. Li, H. Wang, L. Zhang, and W. Fan, "Image reconstruction of electrical resistance tomography based on image fusion," 2011 IEEE Int. Instrum. Meas. Technol. Conf., pp. 1–5, 2011. https://doi.org/10.1109/imtc.2011.5944232
50. H. Wang, L. Tang, and Z. Cao, "An image reconstruction algorithm based on total variation with adaptive mesh refinement for ECT," Flow Meas. Instrum., vol. 18, no. 5–6, pp. 262–267, Oct. 2007. https://doi.org/10.1016/j.flowmeasinst.2007.07.004
51. F. Zhang, "Research on exciting-measuring modes and image reconstruction algorithms for electrical tomography," Tianjin University, 2010.
52. J. L. Davidson, R. A. Little, P. Wright, J. Naish, R. Kikinis, G. J. M. Parker, and H. McCann, "Fusion of images obtained from EIT and MRI," Electron. Lett., vol. 48, no. 11, pp. 617–618, 2012. https://doi.org/10.1049/el.2012.0327
53. D. McCormick, J. L. Davidson, and H. McCann, "Conversion of EIT brain images for co-registration," in 13th Int. conf. on electrical bioimpedance and 8th conf. on EIT, 2007, pp. 384–387. https://doi.org/10.1007/978-3-540-73841-1_100
54. X. Chen, J. Li, and H. Wang, "EIT imaging fused with CT slice," IST 2012 - 2012 IEEE Int. Conf. Imaging Syst. Tech. Proc., no. 50937005, pp. 234–238, 2012. https://doi.org/10.1109/ist.2012.6295543
55. X. Y. Chen, H. X. Wang, and J. C. Newell, "Lung Ventilation Reconstruction by Electrical Impedance Tomography Based on Physical Information," 2011 Third Int. Conf. Meas. Technol. Mechatronics Autom., vol. 2, pp. 489–492, 2011. https://doi.org/10.1109/icmtma.2011.409
56. R. Olmi, M. Bini, and S. Priori, "A genetic algorithm approach to image reconstruction in electrical impedance tomography," IEEE Trans. Evol. Comput., vol. 4, no. 1, pp. 83–88, 2000. https://doi.org/10.1109/4235.843497
57. R. Wexler, A. Fry, B. Neuman, "Impedance-computed tomography algorithm and system," Appl. Opt., vol. 24, no. 3, pp. 3985–3992, 1985. https://doi.org/10.1364/AO.24.003985
58. A. Adler and W. R. B. Lionheart, "Uses and abuses of EIDORS: an extensible software base for EIT.," Physiol. Meas., vol. 27, no. 5, pp. S25–S42, 2006. https://doi.org/10.1088/0967-3334/27/5/S03
59. F. S. Lee, Optimum array processing, vol. 35, no. July. John Wiley and Sons, 2008.
60. S. Manohar, A. Kharine, J. C. G. van Hespen, W. Steenbergen, and T. G. van Leeuwen, "The Twente Photoacoustic Mammoscope: system overview and performance.," Phys. Med. Biol., vol. 50, no. 11, pp. 2543–57, 2005. https://doi.org/10.1088/0031-9155/50/11/007
61. E. A. Thompson, J. Xiang, and Y. Wang, "Frequency-spatial beamformer for MEG source localization," Biomed. Signal Process. Control, vol. 18, pp. 263–273, 2015. https://doi.org/10.1016/j.bspc.2015.01.004
62. L. Swindlehurst, B. D. Jeffs, G. Seco-Granados, and J. Li, Applications of array signal processing, no. Ml. Elsevier, 2014.
63. D. Van Veen and K. M. Buckley, "Beamforming: a versatile approach to spatial filtering," IEEE ASSP Mag., vol. 5, no. April, pp. 4–24, 1988. https://doi.org/10.1109/53.665
64. E. J. Bond, X. Li, S. C. Hagness, and B. D. Van Veen, "Microwave imaging via space-time beamforming for early detection of breast cancer," IEEE Trans. Antennas Propag., vol. 51, no. 8, pp. 1690–1705, 2003. https://doi.org/10.1109/TAP.2003.815446
65. Cao and A. Nehorai, "Tumor localization using diffuse optical tomography and linearly constrained minimum variance beamforming," Opt. Express, vol. 15, no. 3, pp. 896–909, 2007.
66. C. S. Lengsfeld and R. A. Shoureshi, "System and method for beamforming in soft-field tomography," US 2013/0109962 A1, 2008.
67. P. Lafortune and R. Aris, "Linearly constrained minimum variance spatial filtering for localization of conductivity changes in electrical impedance tomography," Int. J. Numer. Methods Biomed. Eng., vol. 28, no. 1, pp. 72–86, 2012. https://doi.org/10.1002/cnm.1494